

Evaluation of porous silicon carbide monolithic honeycombs as volumetric receivers/collectors of concentrated solar radiation

Christos C. Agrafiotis^{a,*}, Ilias Mavroidis^{a,1}, Athanasios G. Konstandopoulos^{a,**}, Bernard Hoffschmidt^{b,2}, Per Stobbe^c, Manuel Romero^d, Valerio Fernandez-Quero^e

^a*Aerosol and Particle Technology Laboratory, Centre for Research and Technology—Hellas, Chemical Process Engineering Research Institute, P.O. Box 361, Thessaloniki 57001, Greece*

^b*German Aerospace Center/DLR, Institute of Technical Thermodynamics—Solar Research, 51170 Cologne, Germany*

^c*Stobbe Tech Ceramics A/S, Vejlemosevej 60, DK-2840 Holte, Denmark*

^d*Centro De Investigaciones Energéticas, Medioambientales Y Tecnológicas /CIEMAT, Avenida Complutense 22, Madrid, Spain*

^e*Solucar SA, Avenida de la Buhaira 2, E-41018 Sevilla, Spain*

Received 24 July 2006; accepted 20 October 2006

Available online 12 December 2006

Abstract

Porous monolithic multi-channeled silicon carbide (SiC) honeycombs employed as open volumetric receivers of concentrated solar radiation, were evaluated with respect to their porous structure and thermomechanical properties before and after long-time operation. Proper “tuning” of porosity, pore size distribution and microstructure can provide SiC honeycombs with improved mechanical properties (higher bending and compressive strength) in the “as-manufactured” state. Exposure under solar irradiation was found to affect both their pore structure and their mechanical characteristics. During the first stages of exposure, a re-structuring of the porous structure takes place shifting the mean pore size to higher values and slightly decreasing the total porosity; this re-structuring ceases after some “characteristic” exposure time. After solar exposure the honeycombs become harder and exhibit significantly higher compressive strength. Extension of anticipated lifetime can be achieved by materials with enhanced mechanical properties like silicon-infiltrated (siliconized) SiC.

© 2006 Elsevier B.V. All rights reserved.

Keywords: Solar thermal collectors; Volumetric receivers; Honeycombs; Silicon carbide; Porous ceramic materials

1. Introduction

The combination of high gas flow rates and elevated temperatures encountered in applications such as automotive catalysis, catalytic combustion and hot gas cleanup, have established thin-wall multi-channeled honeycomb (monolithic) reactors as the configuration of choice [1,2]. Advantages offered by ceramic honeycombs include thin

walls, high geometric surface area and, therefore, good gas–solid contact, accommodation of high gas flow rates combined with low-pressure drop and good mass transfer performance. Further benefits can be gained from special material properties such as thermal shock resistance and mechanical strength; for instance, high temperatures can be tolerated with the use of ceramic materials with high melting point and excellent thermal shock resistance such as cordierite or silicon carbide (SiC).

SiC-based ceramics in particular [3,4] demonstrate superior thermal properties and can be coated with a variety of traditional and novel techniques [5,6], advantages that can be employed for other high-temperature applications such as exploitation of solar energy. The enhanced absorbance of SiC due to its naturally black colour coupled with its high thermal conductivity enables

*Corresponding author. Tel.: +30 231 049 8198; fax: +30 231 049 8190.

**Also to be corresponded to.

E-mail addresses: chrisagr@cperi.certh.gr (C.C. Agrafiotis), agk@cperi.certh.gr (A.G. Konstandopoulos).

¹Present address: Hellenic Ministry for the Environment, Physical Planning and Public Works, 15 Amaliados Street, Athens, Greece.

²Present address: Solar-Institut Julich, Heinrich-Mussmann Street 5, D-52428 Julich, Germany.

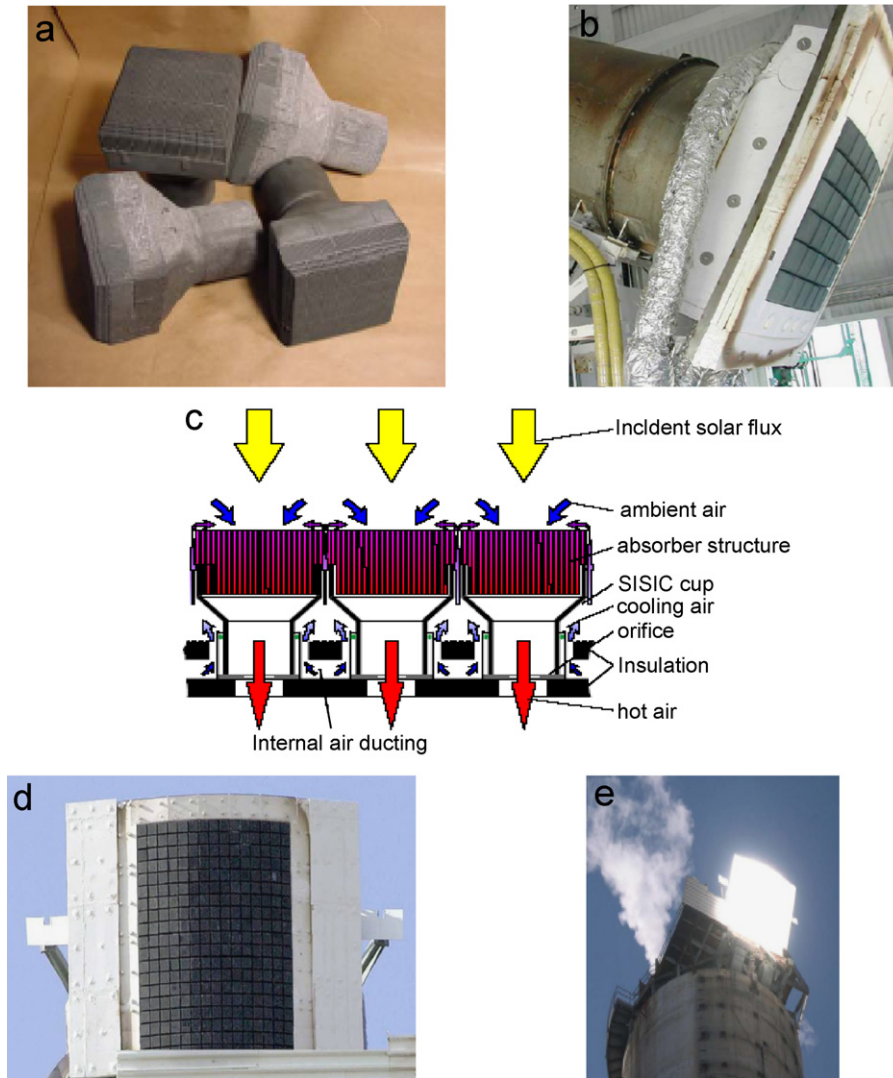


Fig. 1. (a) SiC (125×125 mm) volumetric receiver honeycomb units, (b) modular assembly of the SOLAIR-200 kW receiver, (c) assembly structure and operation principle of receiver modules [10,12], (d) the assembled SOLAIR-3 MW receiver on top of the solar tower and (e) the SOLAIR-3 MW receiver in operation [12].

the collection of solar heat and the effective heating of gases inside the honeycomb channels [7–9]. The heated air can then be directed to a steam turbine for the generation of steam and subsequent production of energy in an integrated solar thermal power plant. This concept of volumetric solar thermal collectors/heat exchangers has been put forth through the project SOLAIR (Advanced Solar Volumetric Air Receiver for Commercial Solar Tower Power Plants-ERK6-CT-1999-00021), aiming to develop, qualify and demonstrate this new technology and promote its installation in the next generation European solar power tower plants. The main objective was to develop an efficient, low-cost simple ceramic solar absorber (Fig. 1a), that can provide high solar concentration, longer material lifetime, stability at high temperatures and—most important—an entirely “modular” design concept: the solar collector/heat exchanger is comprised by a matrix of smaller honeycomb modules providing for

maximum system functionality with respect to minimization of mechanical and thermal stresses, as well as ease of maintenance and replacement of damaged parts. Last but not least, this “modularity” allows for easy scale-up of the absorber concept, from 200 to 3000 kW and upwards [10,11]. The first results were promising: a 200 kW assembly comprising 36 SiC monoliths could act as effective collector of solar heat and achieve temperatures in excess of 1100°C providing air of temperatures around 700°C (Fig. 1b and c). The concept has been successfully scaled up to a 3 MW unit consisting of 270 honeycombs producing steam (Fig. 1d and e) [12].

The present work is concerned with the evaluation of a variety of re-crystallized SiC (abbreviation: reSiC) materials with respect to pore structure and thermomechanical properties both in the “as-manufactured” state as well as after prolonged operation as solar thermal collectors under solar irradiation. The goal was to understand the

phenomena that take place under solar irradiation and increase the lifetime of exposed receiver elements. In addition, an alternative material, silicon-metal-infiltrated SiC (abbreviation: siSiC) known to exhibit superior mechanical properties and oxidation resistance was also explored to meet the demands for prolonged receiver lifetime.

2. Experimental

The first series of laboratory tests were performed on six kinds of as-manufactured SiC honeycombs produced by Stobbe Tech Ceramics, Denmark (Fig. 1a) by extrusion and subsequent firing: five made of reSiC (hereafter denoted as reSiC Nos. 0–4) and one made of siSiC, all having cell density of 90 channels per square inch (c.p.s.i.). Structural characterization was performed on crashed samples in the form of powders by X-ray diffraction analysis (XRD) using a Siemens D-500 Kristalloflex X-ray powder diffractometer and Cu-K_α radiation. Microscopic investigations were performed with a scanning electron microscope (SEM) (JEOL-6400) coupled with EDS X-ray microanalysis (Link ISIS 300, Oxford Instruments). The samples were characterized with respect to porosity and pore size distribution with mercury porosimetry (Quantachrome Autoscan 500 porosimeter). The weight loss of the samples as a function of temperature was studied with thermo-gravimetric analysis combined with differential scanning calorimetry (TGA/DSC) with a T.A. Instruments model SDT2960 thermobalance; samples were heated in oxidative environment (air flow), from 200 to 1500 °C with a ramp of 20 °C/min.

Two types of mechanical strength tests were conducted, compressive and 4-point bending, on an Instron 8562 testing device. Specimens 3 × 3 channels × 6 cm long were sectioned from the honeycomb modules for the 4-point bending tests and 6 × 6 channels × 3 cm long for the compression tests (Fig. 2a) with the aid of a Struers Labotom-1 cutting instrument. All specimens were ground and polished with SiC paper before the mechanical tests. The crosshead speed (constant) was 0.5 mm/min for the compression and 0.2 mm/min for the 4-point bending tests. Sketches of the specimen-support-load application configuration together with the indication of the direction of the applied load with respect to the honeycomb channels as well as the respective cross-section specimen areas are shown in Fig. 2b–e for both kinds of mechanical tests (compression and 4-point bending). The thickness of the channel walls (*t*) was 0.80 mm and the channel width (a) 2 mm.

Specimens from the five reSiC materials were treated in the solar furnace of DLR in Cologne, Germany, for 2000 cycles with a fluctuating solar load of up to 2 MW/m², achieving absorber body temperatures between 220 and 1300 °C [10]. After this treatment, the five samples were subjected to the same microstructural (XRD, SEM, TGA, porosimetry) and mechanical characterizations with the

“as-manufactured” ones, in order to evaluate the effect of solar treatment on the various materials and select the most proper one for subsequent scale-up and testing on the solar platform.

Thirty-six square honeycomb pieces with dimensions 125 × 125 mm (Fig. 1a) manufactured from the most promising reSiC material as identified through these first series of laboratory characterizations, were assembled to the SolAir-200 kW prototype receiver (Fig. 1b) that was installed on the solar platform in Almeria, Spain. The incident solar radiation was reflected by the heliostat field and concentrated on the SiC absorbers with an average flux density of 0.5 MW/m². The test campaign began on March 2002 lasting for 50 operation days and accumulating 182 operation hours providing hot air of a temperature above 700 °C [11,12]. Two reSiC receiver pieces exposed in the solar platform for 94.2 and 186 h, respectively (Fig. 3) were removed for evaluation. In order to comparatively evaluate the efficiency of siSiC absorbers at the same conditions, the 18 cups from the upper half of the receiver (Fig. 3) were replaced with siSiC receivers that operated for 104 h; thereafter an exposed siSiC receiver piece was removed for evaluation. The same characterization tests were performed on the exposed samples in order to identify the effects of solar radiation and exposure time on the receiver element properties.

3. Results and discussion

3.1. Tests on non-exposed (“as-manufactured”) receiver elements

3.1.1. Scanning electron microscopy

The morphologies of two representative “as-manufactured” reSiC samples (Nos. 2 and 4) and of a siSiC sample are compared in Fig. 4 (left column). The difference between the two reSiC samples can be clearly observed: SiC grains of similar size have been employed for the manufacture of both, but a binding phase is employed in the case of reSiC No. 4. This binding phase occupies some of the void space between the SiC grains reducing the intergranular porosity; however, a residual porosity still exists, not only between the large grains but also within the binding phase itself (Fig. 4c). Among the five reSiC types, only type reSiC No. 4 contains a binder phase—the microstructures of types reSiC Nos. 0, 1 and 3 look similar to that of reSiC No. 2 but are not included in Fig. 4 for reasons of brevity. The microstructure of siSiC (Fig. 4e) is entirely different: elongated silicon grains can be observed occupying most of the void space between the SiC grains and reducing significantly the inter-granular porosity.

3.1.2. Porosity and pore size distribution

The mercury porosimetry curves (cumulative and differential) for all “as-manufactured” SiC samples are shown in Fig. 5 (top row). The porosity and mean pore size values are summarized in Table 1 where they are compared

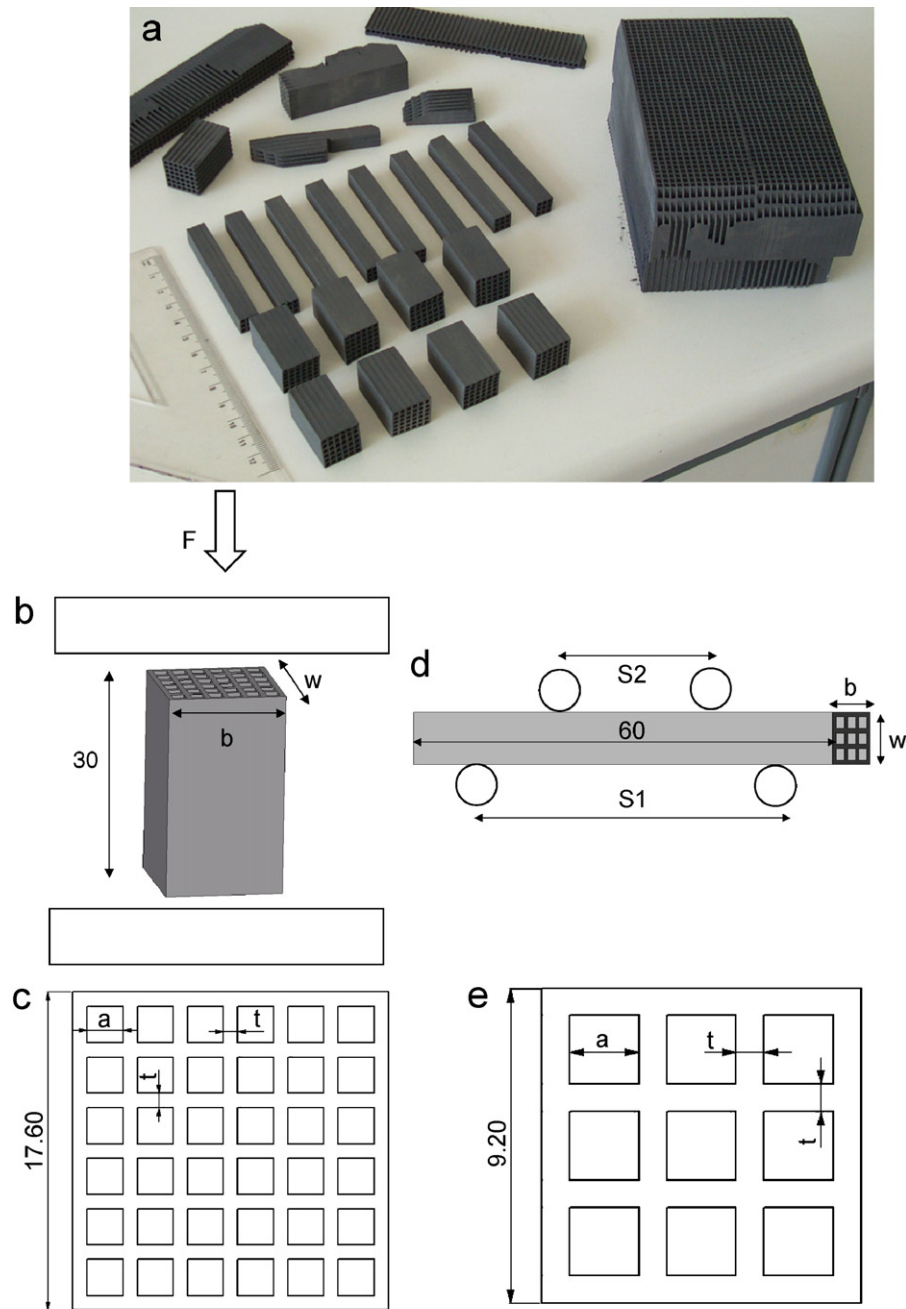


Fig. 2. (a) Specimens sectioned from a volumetric receiver module unit for 4-point bending and compression tests; (b) and (c) compression, (d) and (e) 4-point bending: sketches of direction of applied load with respect to the honeycomb channels and respective cross-section specimen areas.

to the respective values after exposure to solar irradiation (see discussion below). The porosity and mean pore size values of the “as-manufactured” samples are in qualitative agreement with the SEM observations. The pore size distribution curves show the presence of macropores with diameters corresponding to the pores between the SiC particles. The porosity of the “as-manufactured” reSiC samples can be “tuned” from 36% to 44% and their mean pore diameter from 6 to 26 μm . reSiC No. 4 has the lowest porosity (36% similar to that of

reSiC No. 2) and in addition significantly lower mean pore size (6 μm versus 12–26 μm) than all other reSiC parts. It also exhibits a higher percentage of smaller-size pores around 1 μm in diameter (Fig. 5) that clearly correspond to pores within the binding phase. siSiC honeycombs are much denser than reSiC ones: their porosity is almost an order of magnitude lower—3.8% versus 36%. Their mean pore size is around 35 μm , a fact indicating that some inter-granular space has not been infiltrated with Si.

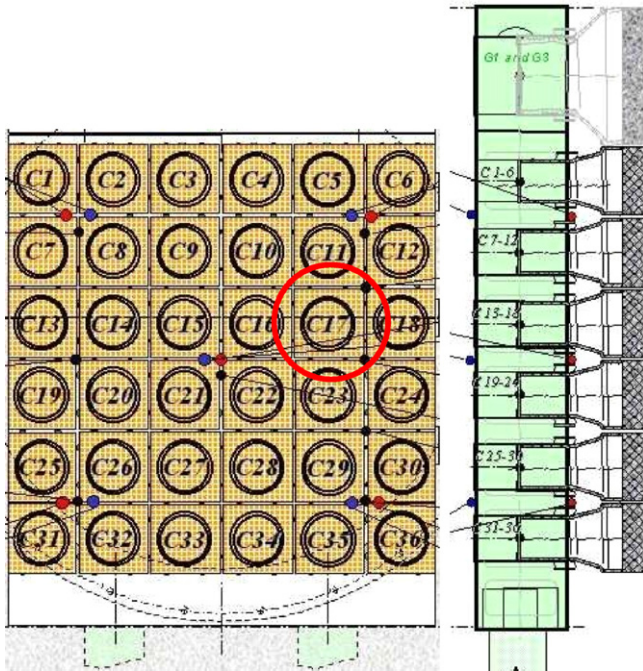


Fig. 3. Front and side schematic of the absorber cups and location of the sample removed after 94.25 h of operation on the receiver (no. C17).

3.1.3. Mechanical tests

The average compressive and bending strength values of all as-manufactured reSiC varieties are compared in Fig. 6. It should be noted that the values shown in Fig. 6 for compression strength are calculated based on the “nominal” specimen area (i.e. referring to Fig. 2, considering the full square-shaped section of the specimens $w \times b$), as follows:

$$\sigma_c = \frac{F_{\max}}{wb}, \quad (1)$$

where F_{\max} is the maximum load.

Four-point bending strength values (modulus of rupture—MOR) are again calculated as if the specimen was a solid rectangular bar, from the formula [13]:

$$\sigma_{(\text{MOR})} = \frac{MC}{I_{xx}}, \quad (2)$$

where, I_{xx} is the second moment of inertia of the cross-sectional area of the bar,

$$I_{xx} = \frac{bw^3}{12}. \quad (3)$$

C is the distance from the neutral axis to the bottom of the bar (i.e. the half-thickness of the bar) and M is the bending moment, which is equal to (Fig. 2d)

$$M = \frac{F_{\max}}{2} \frac{(S_1 - S_2)}{2}. \quad (4)$$

Thus, the final equation for the calculation of the 4-point bending strength is

$$\sigma_{(\text{MOR})} = \frac{3(S_1 - S_2)F_{\max}}{2bw^2}. \quad (5)$$

Sample reSiC No. 4 that exhibits the lowest porosity and mean pore size among the reSiC parts, also exhibits both the highest bending and compressive strength values (17.8 and 25.95 MPa, respectively). The mechanical properties of the reSiC material No. 4 are compared to those of siSiC in Fig. 7 for all the specimens tested from each material. “As-manufactured” siSiC specimens showed 4 times higher average compressive strength—118.11 versus 25.95 MPa—and 3 times higher average bending strength—56.17 versus 17.8 MPa—than the “strongest” “as-manufactured” reSiC (No. 4) specimens.

Compressive and 4-point bending strengths reported in the literature for SiC materials are much higher; compressive strength values in the range 4200–4600 MPa have been reported [14,15] whereas bending (flexural) strength values reported, range between 260 and 480 MPa [16–20] depending on the type of SiC material examined and its density. It should be noted, however, that such values are obtained from mechanical tests of almost fully dense samples (relative densities ~ 96 –99% of theoretical). The present study involves tests on honeycomb-like specimens that not only have a high percentage of “open frontal area” but the channel walls are themselves porous. A first “correction” can be implemented by taking into account only the walls solid surface i.e. “subtracting” the open frontal area of the flow channels both in the evaluation of the compressive stress as well as in the evaluation of the bending moment and the respective bending strength. The values of the compressive and 4-point strength values calculated this way, are on the average 30–35% higher in the case of compression and 60–70% higher in the case of 4-point bending, than these calculated from Eqs. (1) and (5).

For the description of the mechanical behaviour of highly porous cellular solids like honeycombs and foams, semi-empirical equations like the following:

$$\frac{\sigma_c}{\sigma_{ys}} = C_2 \left(\frac{\rho_c}{\rho_s} \right), \quad (6)$$

have been proposed [21] (the particular equation is proposed for the case of axial compression of honeycombs) that correlate the strength of the cellular structure σ_c with that of the fully dense material σ_{ys} and their respective densities ρ_c , ρ_s . C_2 is an experimental constant that can be determined from experiments on specimens with different porosity (density) values. However, since in the present study, the mechanical tests have been performed on specimens of similar porosity sectioned from the same honeycomb such an approach is not possible.

A better ground of comparison is vs. values reported in the literature determined from mechanical tests performed on honeycomb specimens sectioned from diesel particulate filters (DPFs) made of SiC materials—tests that are common among DPF manufacturers. Various manufacturers of such filters have reported values of compressive strength between 6 and 50 MPa and of bending strength in the range 6–40 MPa for SiC honeycombs [22–24]. The variation is due to the different kinds of SiC employed

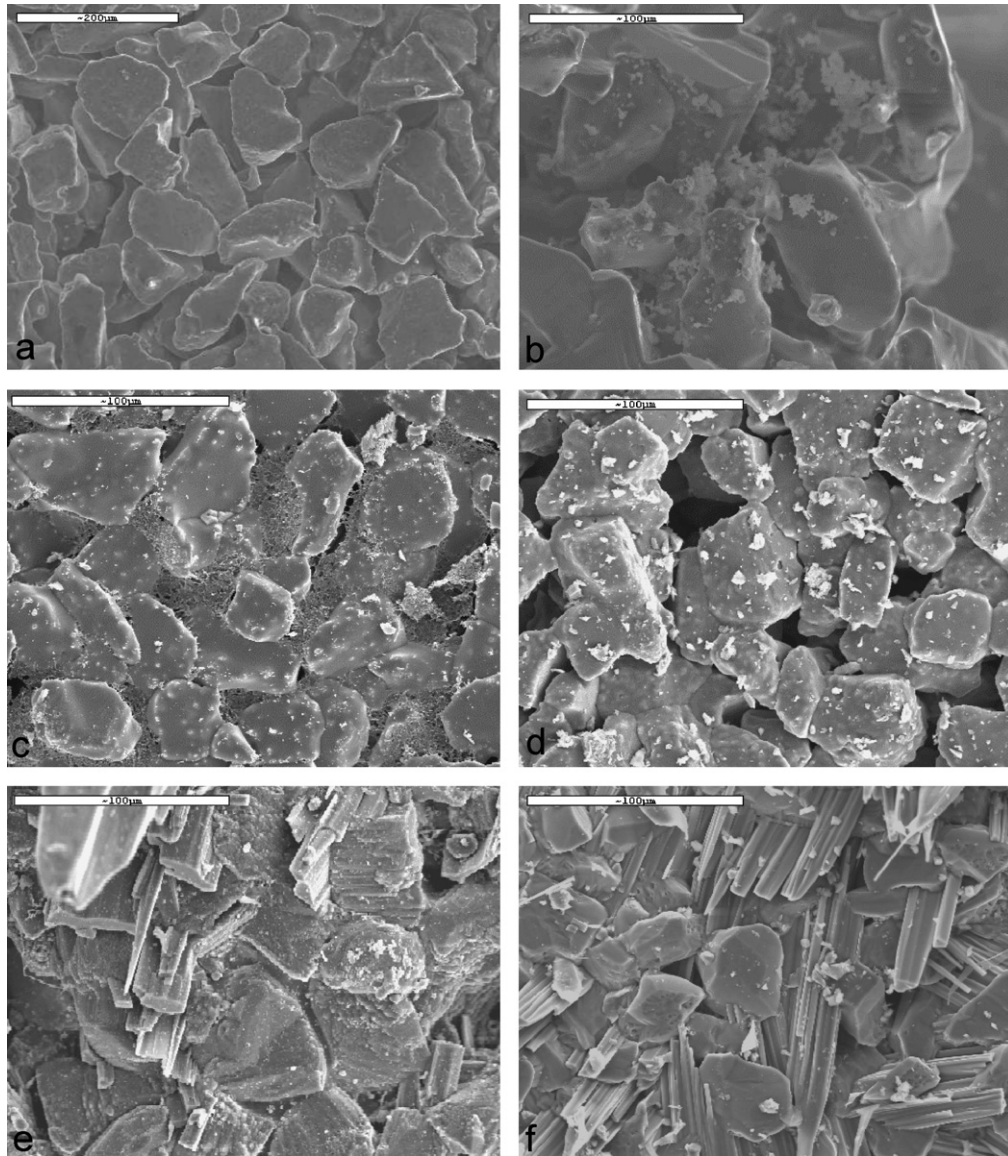


Fig. 4. SEM photographs of representative “as-manufactured” (left) and exposed to solar irradiation (right) samples: (a) reSiC No. 2 “as-manufactured”, (b) reSiC No. 2 exposed in the solar furnace, (c) reSiC No. 4 “as-manufactured”, (d) reSiC No. 4 exposed in the solar platform, (e) siSiC “as-manufactured”, (f) siSiC exposed in the solar platform.

(recrystallized, reaction-sintered or siliconized) and due to differences among the materials’ porosity (typically between 40% and 58%) and the number of c.p.s.i. Strength values of similar magnitude have been reported for tests on honeycomb specimens from other ceramic materials employed for the manufacture of DPFs: compressive strength of 10 MPa and bending strength of 2.6 MPa have been reported for cordierite [25], compressive strength of 18 MPa and bending strength of 5.1 MPa have been reported for silicon nitride [26] and bending strength of 30 MPa for acicular mullite 200 c.p.s.i. DPF specimens [27]. It can be concluded that the SiC honeycombs examined in the present study, exhibit mechanical strength properties comparable to the highest ones reported for commercial honeycombs.

3.1.4. Thermo-gravimetry/differential scanning calorimetry

Typical TGA/DSC curves are shown in Figs. 8 and 9. In Fig. 8a, the weight loss curves of all tested samples, as-manufactured (plain lines) and exposed (bulleted lines), are compared. All as-manufactured reSiC samples exhibit similar behaviour: a weight loss between 600 and 800 °C associated with an exothermic reaction (shown for the case of reSiC No. 4 in Fig. 8b). The most plausible explanation is its association with the oxidation of possible residues of free carbon in the as-manufactured samples to gaseous CO₂. At temperatures above 1000 °C an increase in weight is observed accompanied by an endothermic peak (Fig. 8b for reSiC No. 4) that most likely corresponds to the oxidation of SiC to SiO₂. Above 1300 °C, this oxidation becomes more intense. reSiC No. 4 not only suffers

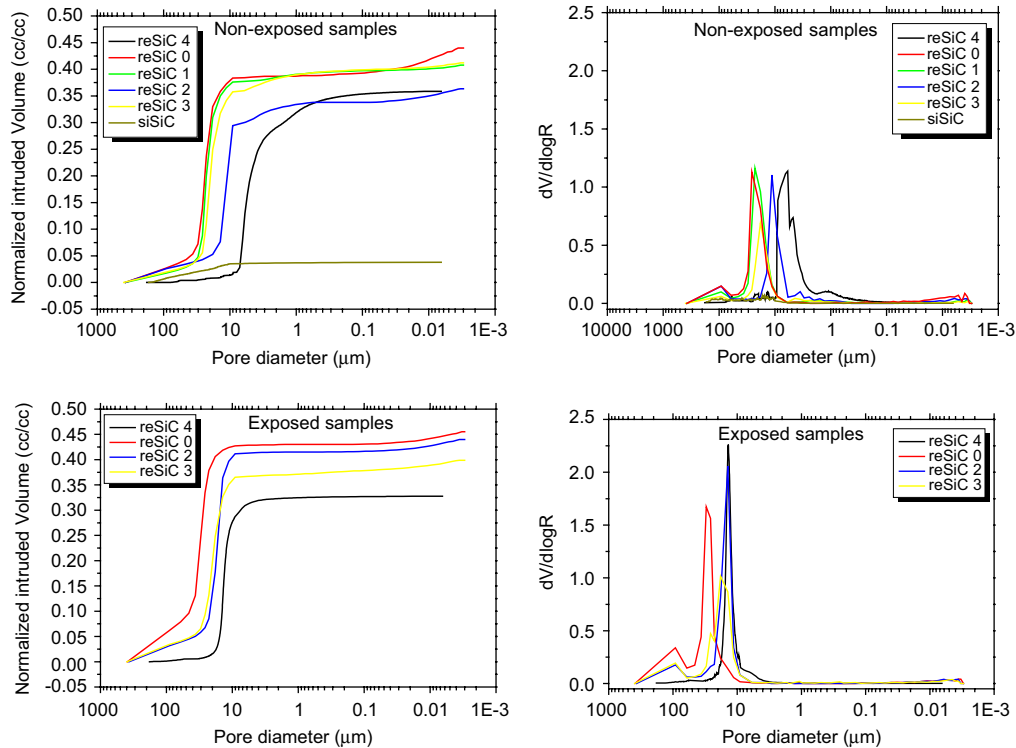


Fig. 5. Hg porosimetry cumulative (left) and differential (right) pore size distribution curves of “as-manufactured” reSiC and siSiC samples (first row) and reSiC samples exposed in the solar furnace (second row).

Table 1
Porosity and mean pore diameter of SiC samples, as-manufactured and after exposure to solar irradiation

Sample	Porosity (%)		Mean pore diameter (μm)	
	As-manufactured	Exposed	As-manufactured	Exposed
reSiC 0	44.0	45.5	26	30.5
reSiC 1	40.8		23	
reSiC 2	36.3	44.0	12	13.6
reSiC 3	41.2	39.9	18	18.0
reSiC 4	35.9	33.4 (94.2 h)	6	13.6 (94.2 h)
		33.0 (186 h)		16.0 (186 h)
siSiC	3.8		35	

the least weight loss from all other reSiC samples (0.08%) but starts to oxidize (gain weight) at slightly higher temperatures (the flat region of the weight loss curve is extended to higher temperatures). It should be noted, however, that the weight losses for all reSiC samples are less than 1%. siSiC exhibits the most stable behaviour in the as-manufactured state: it does not suffer any weight loss up to 800 °C and only a minute total weight loss (<0.02%) upon further heating to 1300 °C ; however, it can be clearly seen from the respective heat flow curves shown in Fig. 9, that above 1400 °C an intense endothermic process (melting of metallic free Si, its melting point being 1410 °C) takes place in contrast to the reSiC sample.

Based on the results above, among the reSiC varieties, reSiC No. 4 was selected as the construction material for the manufacture of the (125 × 125 mm) honeycomb pieces to be assembled to the 200 kW prototype solar receiver due to its superior mechanical properties and oxidation resistance.

3.2. Tests on exposed receiver elements

As already mentioned, exposed elements are distinguished in two categories: samples exposed in the solar furnace in Cologne, Germany (reSiC Nos. 0–4), and samples exposed on the 200-receiver in the solar platform at Almeria, Spain (reSiC No. 4, siSiC). The SolAir-200 receiver prototype operated during 50 operation days, accumulating in the first tests stage, 186 operation hours with 36 reSiC No. 4 ceramic absorber elements. In order to evaluate the efficiency of siSiC absorbers and compare them with the reSiC ones under the same conditions, the 18 cups from the upper half of the receiver were replaced with siSiC absorbers that operated for 100 h. The operation hours accumulated at the various temperature levels during the test campaigns for both absorber materials (reSiC No. 4 and siSiC) are shown in Fig. 10a.

Two reSiC 4 receiver pieces exposed in the solar platform for 94 and 186 h and one siSiC piece exposed for 104 h were evaluated. No mechanical damages or visible cracks were observed on the samples. The samples exhibited a change in colour: they became lighter than the non-exposed ones

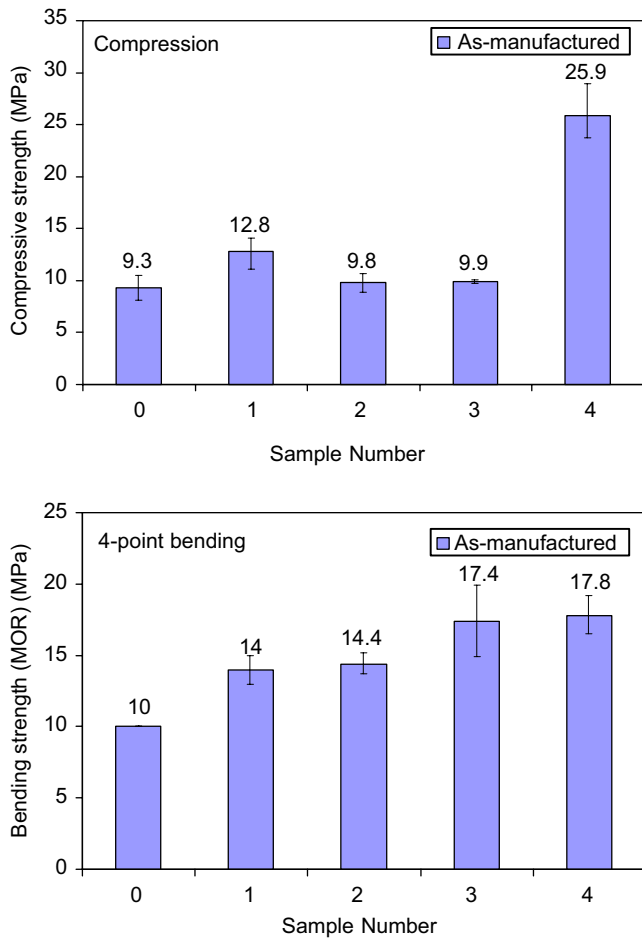


Fig. 6. Comparison of average compressive (top) and four-point-bending (bottom) strength among as-manufactured reSiC varieties.

and exhibited some iridised spots close to the top entrance rim (Fig. 10b).

3.2.1. Scanning electron microscopy/EDS/XRD

The morphology of the exposed samples is compared to that of the respective “as-manufactured” ones in Fig. 4. In the two specimens from samples exposed in the solar platform, SEM analysis shows clearly small “foreign” particles (e.g. sand, debris etc. as corroborated via EDS that showed the presence of Fe, Ni, Cu and other metals in smaller quantities) deposited on the surface of the SiC grains. In the case of reSiC No. 4 after solar irradiation (Fig. 4d), the binding phase has either dissolved within the large SiC grains and/or some material has evaporated leaving behind traces of fine white powder, most likely SiO₂.

The XRD spectra of “as-manufactured” and exposed reSiC No. 4 samples are compared in Fig. 11 and the respective EDS spectra for the case of reSiC No. 4 are shown in Fig. 12. XRD (Fig. 11) identifies SiC as the main constituent of both “as-manufactured” and exposed samples. It is known that SiC exhibits many polytypes, based on the tetrahedral coordination of carbon and silicon. The 3C type of cubic structure is accepted as the

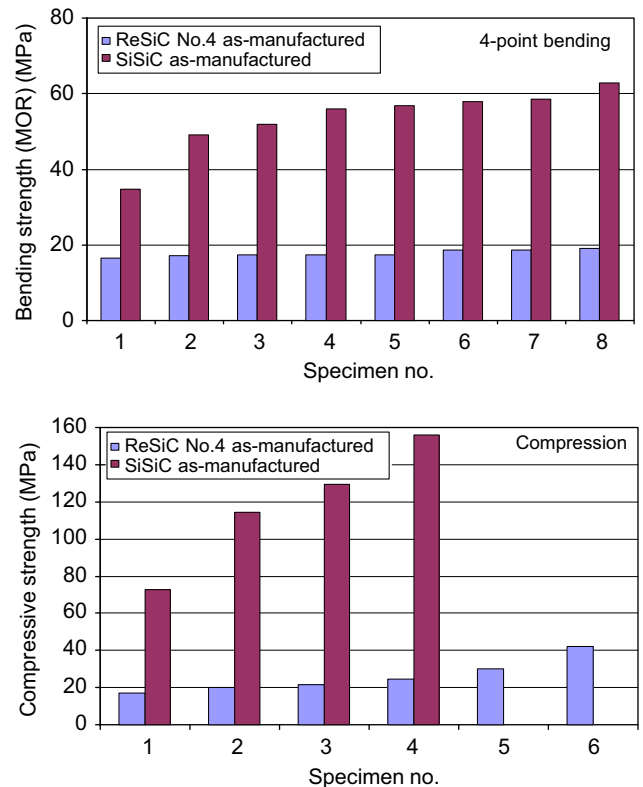


Fig. 7. Comparison of 4-point-bending (top) and compressive (bottom) strength between non-exposed reSiC 4 and siSiC samples.

low-temperature stable form up to 2100°C; at this temperature is converted to the hexagonal form 6H [28]. Both “as-manufactured” reSiC and siSiC consist predominantly of a mixture of 3C and 6H phases. ReSiC contains also traces of the 4H polytype, whereas the peaks corresponding to free Si are also evident for the case of “as-manufactured” siSiC (Fig. 11b), their intensity being significantly reduced after exposure to solar radiation. Allotropic transformations of SiC take place during high-temperature exposure of reSiC No. 4 indicated by the change in the relevant intensity of the peaks corresponding to the different phases, together with oxidation to SiO₂. The XRD spectrum of exposed reSiC No. 4 indicates only a peak of very low intensity at a diffraction angle of 21.7°, corresponding to cristobalite; however, EDS elemental analysis shows undoubtedly the presence of Oxygen in addition to silicon and carbon in the exposed samples (Fig. 12) in contrast to the non-exposed ones. These observations indicate that the SiO₂ formed is a mixture of amorphous phase and cristobalite, in accordance with previous experimental studies in the literature [29], reporting that in most oxidation experiments SiO₂ first forms an amorphous film and then crystallizes to either cristobalite or tridymite.

3.2.2. Porosity and pore size distribution

The results of mercury porosimetry for all the exposed SiC samples are compared at the same scale to those in the

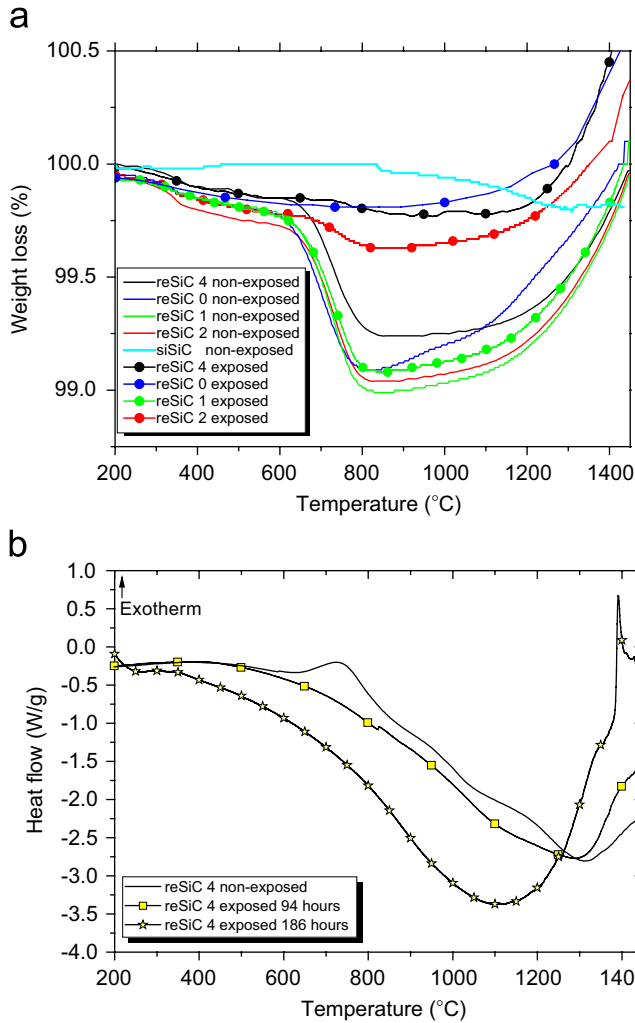


Fig. 8. TGA/DSC results. (a) Weight loss as a function of temperature for non-exposed and exposed reSiC and siSiC samples and (b) heat flow curves for non-exposed and exposed reSiC No. 4.

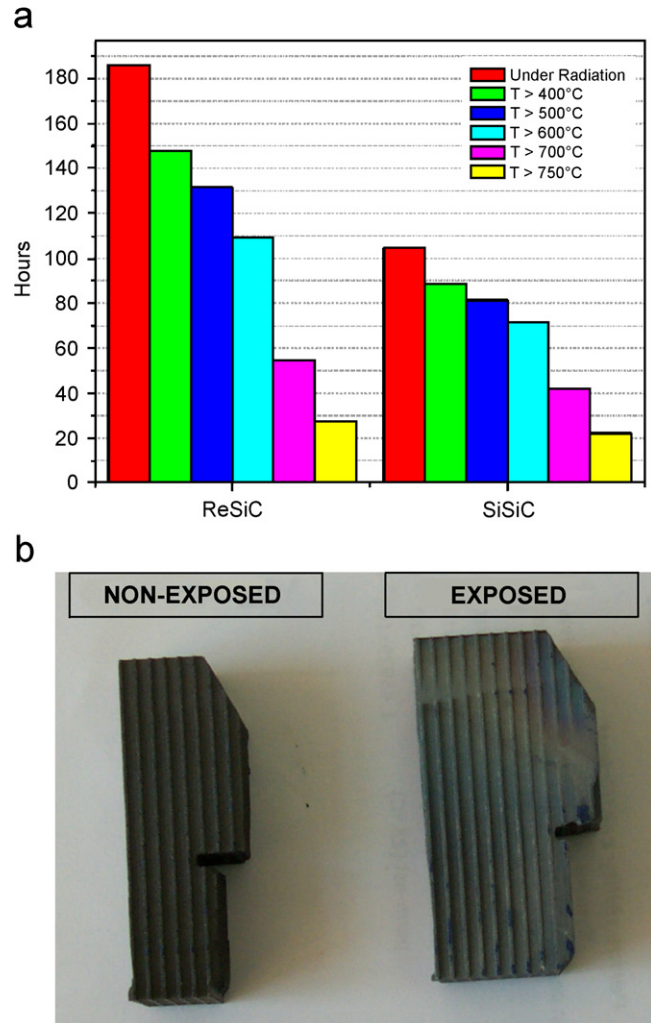


Fig. 10. (a) Summary of accumulated operating hours at different temperature levels for the two kinds of receiver materials and (b) visual comparison between non-exposed and exposed reSiC No. 4 sample.

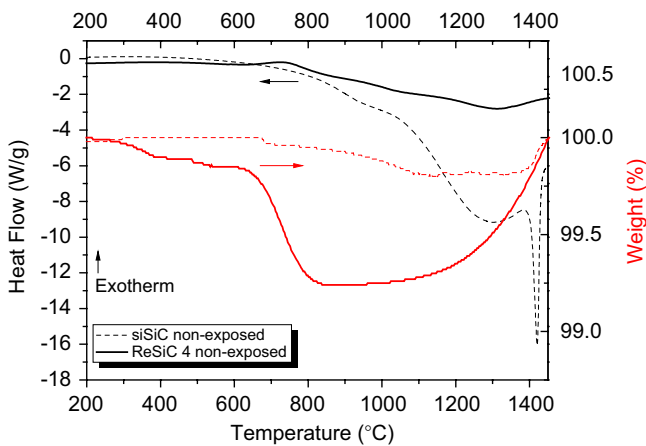


Fig. 9. Comparison of weight loss and heat flow curves (TGA/DSC, respectively) between “as-manufactured” reSiC No. 4 and siSiC.

“as-manufactured” state in Fig. 5. Exposure to solar irradiation has only a minor effect on the total porosity of reSiC samples that practically remains unaffected. How-

ever, the pore size distributions of all samples become narrower and are shifted to higher mean pore values after exposure to solar irradiation, a fact indicating that a restructuring of the porous structure takes place. This is further evidenced by the cumulative and differential pore size distributions for the exposed and non-exposed reSiC No. 4 samples shown in Fig. 13 as a function of exposure time. For this particular sample, a slight reduction in porosity (from 36% to 33%) after exposure to solar irradiation is observed, whereas the pore size distribution narrows significantly and shifts towards a higher mean pore diameter (from 6 to 13.6 μm). This means that after the prolonged exposure under solar irradiation and at the temperatures developed, some of the smaller pores close completely or disappear. The latter is the case with the small pores observed within the binding phase of the non-exposed sample (Figs. 4c and d). The high shift of mean pore diameter towards higher values observed only on samples of reSiC No. 4, provides strong evidence for association with changes that take place mainly in the

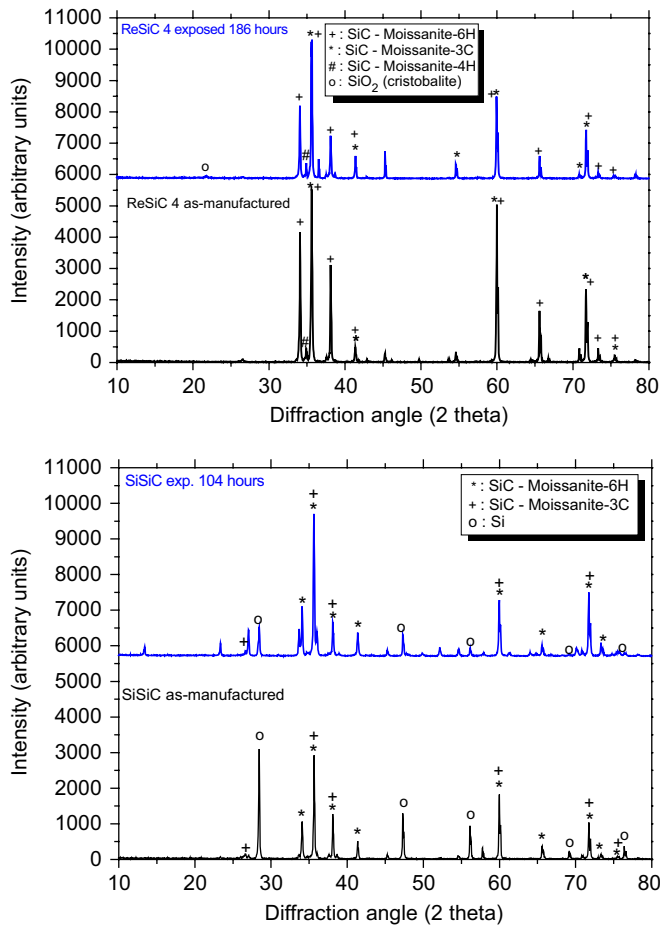


Fig. 11. XRD comparison between “as-manufactured” and exposed in the solar platform samples, for the materials reSiC No. 4 (top) and siSiC (bottom).

binder phase rather than in the structure of the SiC phase itself. The binder phase contains very small grains that are far more susceptible to sintering during exposure under solar irradiation than the much coarser SiC grains. Such small binder grains can sinter to larger ones that are progressively removed from the intergranular pores during exposure or deposit on neighbouring SiC grains. Another possible cause for reduction of total porosity and closing of small pores could be the accumulation of “foreign” particles inside the porous structure of the receivers during operation (as discussed in Section 3.2.1) and their eventual sintering at the high operation temperatures. After a “characteristic” exposure time the pore structure does not change anymore (Fig. 13, bottom): it seems that the specimens “converge” to a “final” pore structure that does not further change with the extension of operation time.

3.2.3. Thermo-gravimetry/differential scanning calorimetry

Exposed samples have already undergone partial oxidation; thus (with the exception of reSiC No. 1) they lose much less weight in the respective TGA experiments (Fig. 8a). The exposed reSiC No. 4 samples do not exhibit the exothermic peak in the temperature range 700–800 °C

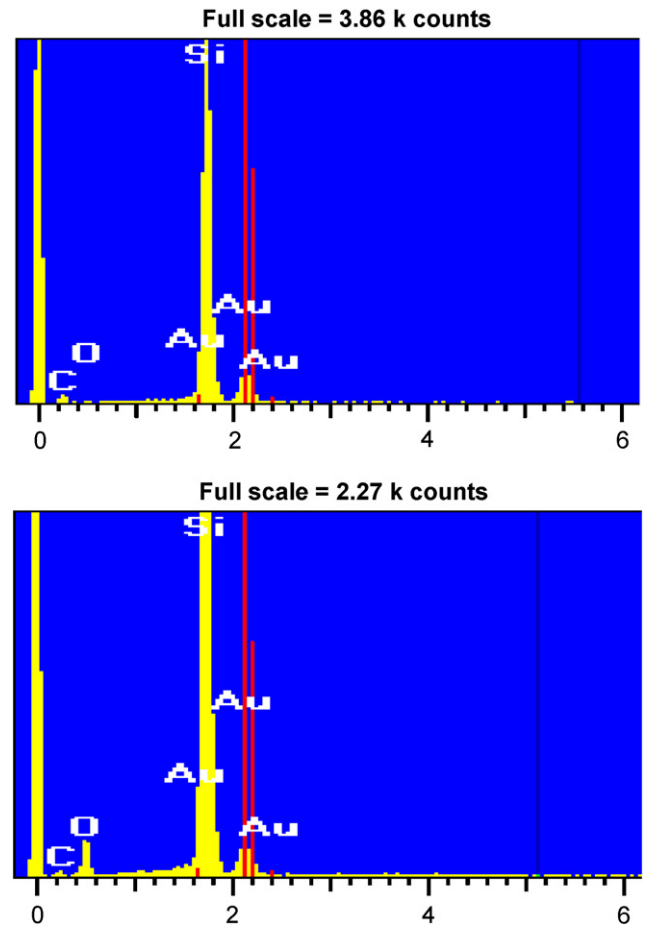


Fig. 12. EDS elemental analysis comparison between “as-manufactured” (top) and exposed reSiC No. 4 (bottom) samples indicating the presence of oxygen in the latter.

in contrast to the non-exposed one (Fig. 8b). They only lose a minute amount of weight up to 1200 °C; thereafter weight gain (oxidation) begins in a similar fashion to that of the non-exposed sample (similar shape of heat flow curves and peaks at the same temperature range). This indicates that the SiO₂ layer that is formed during exposure under solar irradiation protects the SiC particles from further oxidation.

3.2.4. Mechanical tests

Specimens similar to those described in Section 2 were sectioned from the exposed samples, grinded and polished for the bending and compression tests. It should be noted though, that the honeycombs become harder after exposure, and, therefore, more brittle, which makes much more difficult the preparation (sectioning/grinding/polishing) of specimens for the mechanical tests and enhances the possibility for introduction of flaws. The lack of mechanical tests on the exposed siSiC sample is due to the fact that the siSiC honeycombs were so firmly glued to the surrounding siSiC cups that sectioning of “flawless” specimens for mechanical testing was not possible.

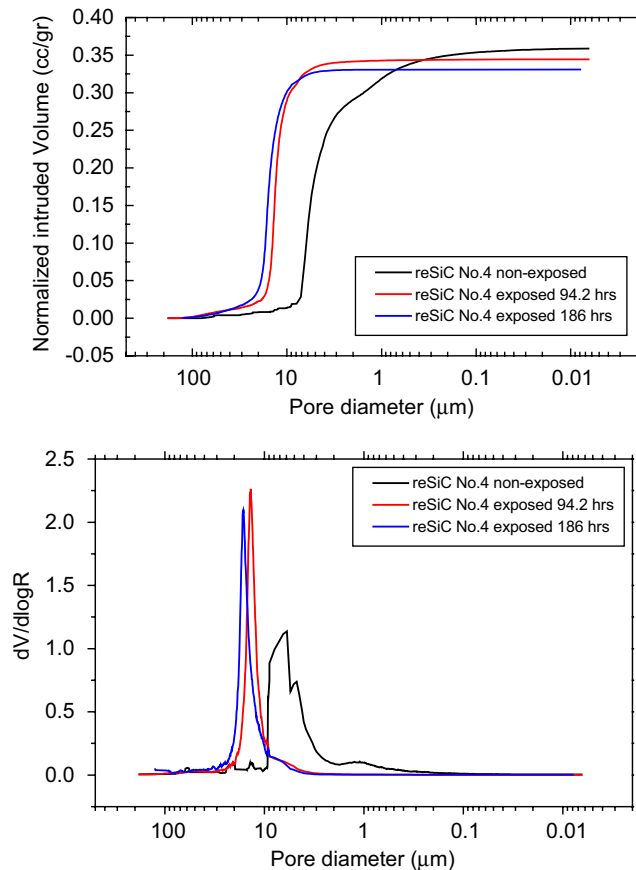


Fig. 13. Hg porosimetry cumulative (top) and differential (bottom) pore size distribution curves of reSiC No. 4 sample exposed in the solar platform, as a function of exposure time.

Four-point bending tests: The location on the reSiC No. 4 monolith exposed for 94.2 h, from where the first batch of specimens for 4-point bending tests was sectioned, is shown in Fig. 14 together with the measured 4-point bending strength values for each specimen. The difficulty in preparing proper specimens can be clearly pointed out: as it can be seen in Fig. 14a, out of the eight specimens that could be sectioned from the same honeycomb “row”, two were damaged during the sectioning process (one marked as No. 1 and one non-marked between specimens 4 and 5). The 4-point bending strength values of specimens Nos. 3–7 are close to each other and higher than the respective values of the non-exposed specimens, whereas that of specimen No. 2 is much lower. Due to this discrepancy, six more specimens were sectioned; the results are summarized as a function of exposure time in Fig. 15a compared to those corresponding to the non-exposed (“as-manufactured”) samples.

For the case of 94.2 h exposure time the exposed specimens can be clearly distinguished in two groups: one of lower strength (≈ 12 MPa) and one of higher strength (≈ 27 MPa) than the non-exposed specimens (≈ 18 MPa). On the contrary for the case of 186 h exposure time, all exposed specimens exhibit higher strength than the

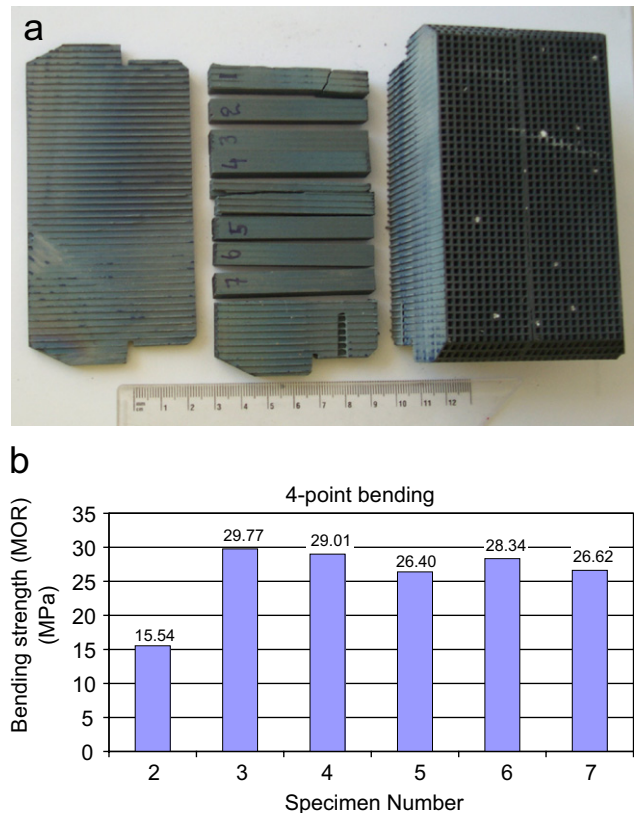


Fig. 14. (a) Position of 6 4-point bending specimens sectioned from the reSiC No. 4 honeycomb exposed for 94.2 h, (b) relevant 4-point bending strength values.

non-exposed specimens. For both cases a wide scatter of strength values (94.2 h: 10–31 MPa, 186 h: 18–51 MPa) can be observed.

These discrepancies among specimens from the same receiver piece occur as a result of non-homogeneous temperature distribution across the honeycomb’s surface. Recent measurements of the air temperature distribution behind such volumetric absorbers [30] point out that very high-temperature gradients across the absorber’s cross-section can be developed. Due to the receiver modules’ operation (Fig. 1c) where the outer edges of each module are exposed to the cooling air stream flowing upwards between the adjacent modules, thermal stresses close to the lateral edges are higher. This could explain the lower strength value of specimen No. 2 and the failure of specimen No. 1 (Fig. 14) during sectioning. Unfortunately, except for the first six specimens the location of the rest on the honeycomb’s area was not marked, thus a detailed two-dimensional “mapping” of bending strength as a function of the location of the specimen on the receiver could not be made.

Even though the number of specimens from both the non-exposed (8 specimens) and the 94.2-h-exposed samples (12 specimens) was not large (it should have been close to 30), two indicative Weibull diagrams were constructed for both cases. The survival probability was estimated using

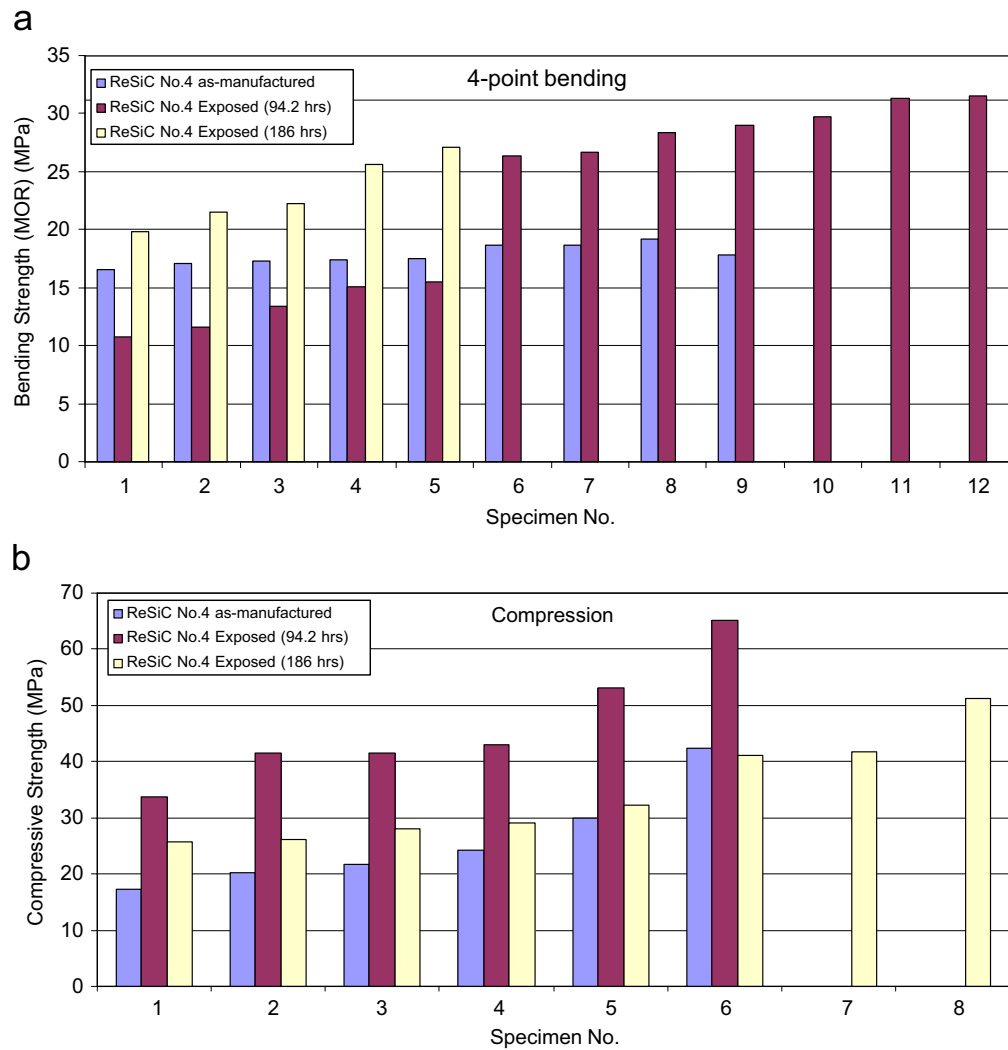


Fig. 15. Comparison of (a) 4-point bending strength and (b) compressive strength, between non-exposed and exposed in the solar platform reSiC No. 4 samples as a function of exposure time.

the formula [13]:

$$S_j = 1 - \frac{n - 0.5}{N}, \quad (7)$$

where N is the number of total specimens, organized from weakest to strongest and given a rank n with $n = 1$ being the weakest specimen. The respective values of the fracture strength and the calculated survival probability are summarized in Table 2. For the case of as-manufactured sample (Fig. 16) it can be seen that the low scattering of the 4-point bending strength values for the specimens leads to the relatively high Weibull modulus of 21.6. All specimens probably failed due to the same mechanism that most likely is due to crack initiation at stress concentration sites such as the square channel corners or pores located near such points, since the fracture is inter-granular and no micro-cracks were observed on the SiC grains under the SEM.

On the other hand, for the case of the exposed sample (Fig. 17a), the high scattering of the 4-point bending strength leads to the low Weibull modulus of 2.7. However,

it is also evident from the graph in Fig. 17a that the exposed specimens can be categorized into two different groups—these two categories are plotted separately in Fig. 17b.

Compressive strength tests: The compressive strength results are shown in Fig. 15b compared to those corresponding to the non-exposed (“as-manufactured”) samples. Despite the significant scatter of values observed among exposed specimens sectioned from the same receiver piece—a scatter that can be attributed to flaws introduced during the specimen preparation process—it can be concluded that compressive strength increases significantly after exposure under solar irradiation. Considering experimental error and data scattering, the trend with exposure time follows that of porosity: after some critical exposure time, where the pore structure does not exhibit further significant change, further solar irradiation exposure time has no significant effect on compressive strength.

To summarize, two processes taking place simultaneously during operation, seem to affect the mechanical

Table 2
Experimental 4-point bending fracture strength of tested “as-manufactured” and exposed reSiC No. 4 specimens and calculated survival probability

Specimen No, <i>j</i>	MOR, σ_j (MPa)	Survival probability, S_j
<i>reSiC No. 4 “as-manufactured”</i>		
1	16.50	0.9375
2	17.10	0.8125
3	17.34	0.6875
4	17.42	0.5625
5	17.45	0.4375
6	18.67	0.3125
7	18.71	0.1875
8	19.18	0.0625
<i>reSiC No. 4 exposed for 94.2 h</i>		
1	10.74	0.9583
2	11.61	0.8750
3	13.40	0.7917
4	15.06	0.7083
5	15.54	0.6250
6	26.40	0.5417
7	26.62	0.4583
8	28.34	0.3750
9	29.01	0.2917
10	29.77	0.2083
11	31.26	0.1250
12	31.51	0.0417

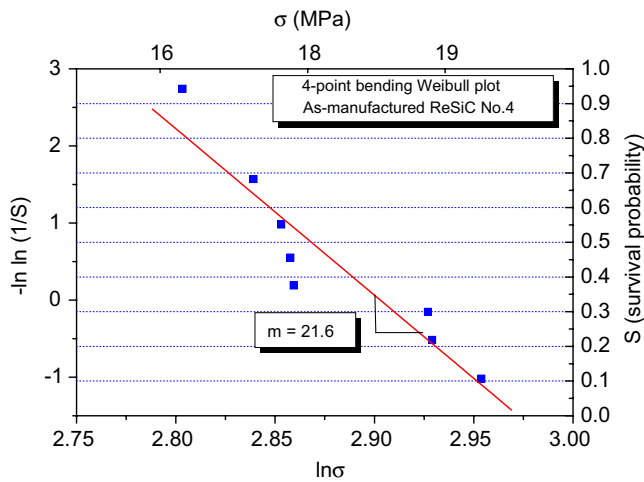


Fig. 16. Weibull diagram from the 4-point bending tests, for the as-manufactured reSiC No. 4 samples.

properties of the receiver honeycombs. In one hand, long-term exposure to solar irradiation is equivalent to a post-sintering process that—as shown from porosimetry data—results in a reduction in porosity and, therefore, an increase on the mechanical strength of the exposed honeycombs. However, the overall reduction in porosity after exposure (from ~36% to 33%) does not seem to be enough to justify an almost two-fold increase on mechanical strength. The increase in strength observed after exposure is more likely associated with changes in the samples’ microstructure during the solar high-temperature treatment. During this

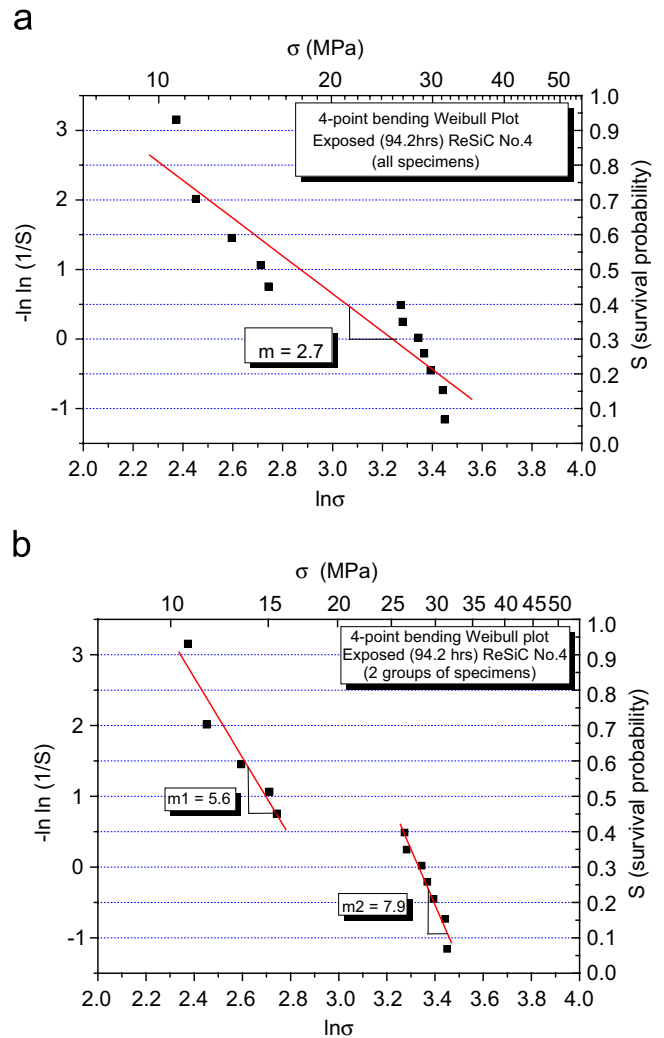


Fig. 17. Weibull diagrams from the 4-point bending tests for the exposed (for 94.2 h) reSiC No. 4 samples: (a) for all specimens plotted together and (b) for the two groups of specimens plotted separately.

treatment, thermal stresses possibly introduced in the samples during the manufacturing process (firing at high temperatures and subsequent cooling to room temperature) are released whereas possible sharp flaw edges originally present in the non-exposed samples are smoothed (crack healing and blunting); all these combined effects can contribute to the observed increase of strength after solar exposure.

On the other hand the non-uniform temperature of the honeycomb during operation results in a thermal stress field across the honeycombs’ cross-section: the outer regions of the receiver are exposed to much higher thermal stresses during operation than its central part. This stress field together with the thermal fatigue-mode-operation (several heating–cooling steps) can result in micro-cracks (Fig. 18) that can deteriorate the mechanical properties. The effect of such micro-cracks can be observed much more clearly in 4-point-bending tests where the lower surface of the specimens is under tension, rather than in compression tests. However, it is not likely that such

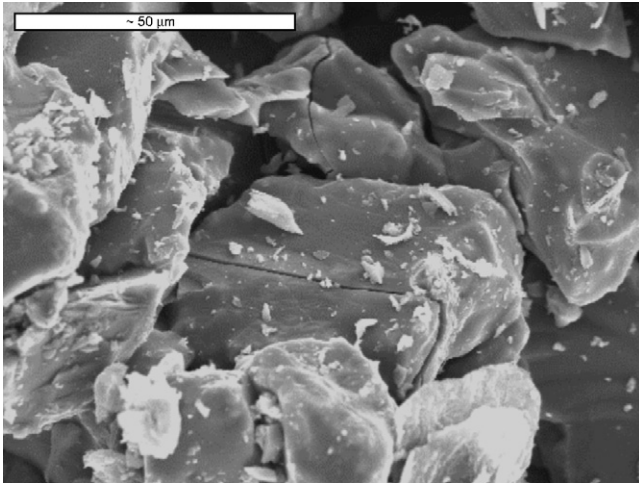


Fig. 18. Cracks observed on specimens from the exposed reSiC No. 4 sample.

intragranular microcracks are the origins of final fracture; as already mentioned for the case of “as-manufactured” materials the fracture of SiC is primarily intergranular and for honeycomb specimens as these tested in the present study, the origins of fracture are most likely the channel corners or the pores located near these points. The difference in bending strength between the two groups in Fig. 17b, should be attributed to the location of the sectioned specimens in correlation to the thermal stress field developed across the honeycomb’s cross-section area.

In addition, on specimens from exposed receivers, 4-point-bending strength values both higher and lower than the respective values of specimens from non-exposed receivers can be observed. Specimens sectioned from the edge areas of exposed receivers can result in lower bending strength values than specimens from non-exposed honeycombs due to the development of microcracks created from intense thermal stresses at these locations; on the other hand specimens from the central areas of exposed receivers can demonstrate higher bending strength than specimens from non-exposed honeycombs, due to the prolonged post-sintering process and the absence of thermal stresses in this central area. Therefore, an operational design that can minimize the thermal stresses across the receiver’s cross-section area and help avoiding the deterioration of the receiver’s mechanical properties is of crucial importance.

4. Conclusions

Porous monolithic honeycombs from a variety of SiC materials and employed as solar volumetric receivers were evaluated with respect to their porous structure and thermomechanical properties before and after long-time operation under concentrated solar irradiation. The results are summarized below:

- Proper “tuning” of porosity, pore size distribution and microstructure can provide reSiC honeycombs with

improved mechanical properties (higher bending and compressive strength) in the “as-manufactured” state.

- Superior properties—4 times higher compressive, 3 times higher bending strength and negligible weight loss due to oxidation—can be achieved with the use of siliconized SiC.
- During the first stages of exposure, a re-structuring of the porous structure takes place: pore size distribution becomes narrower, mean pore diameter shifts to higher values and total porosity decreases slightly. These properties practically cease to vary after some “characteristic” exposure time.
- Exposure under solar irradiation renders the receiver material harder and increases significantly its compressive strength. The non-uniform temperature field across the receiver’s cross-section during operation, induces thermal stresses that can deteriorate the mechanical properties of the receiver modules. Therefore, an operational design that can minimize the development of thermal stresses is essential.
- Surface oxidation of reSiC materials to SiO₂ does occur. Extension of anticipated lifetime can be achieved by the synthesis of more oxidation-resistant SiC materials like siSiC, which, in addition, has superior mechanical properties and an upper limit of operating temperature ($\approx 1400^\circ\text{C}$) much higher than the usual operating temperatures of volumetric receivers.

Due to their good thermomechanical properties, in addition to their use as volumetric solar receivers, such multi-channelled porous honeycombs can be coated with proper catalytic or redox materials, in a configuration similar to that encountered in automobile exhaust catalytic aftertreatment and employed for high-temperature reactions (e.g. water splitting for the production of Hydrogen) opening new perspectives in the area of Solar Chemistry [31,32].

Acknowledgements

The authors would like to thank the European Commission for partial funding of this work, within the Project “Advanced Solar Volumetric Air Receiver for Commercial Solar Tower Power Plants—SOLAIR” (no. ERK6-CT-1999-00021), under the ‘Energy, Environment and Sustainable Development (part b: Energy)’ Programme (1998–2002), and their collaborator in the Project, K. Hennecke from German Aerospace Center/DLR.

References

- [1] R.M. Heck, R.J. Farrauto, Catalytic Air Pollution Control—Commercial Technology, Van Nostrand Reinhold, New York, 1995.
- [2] J.W. Geus, J.C. van Giezen, Catal. Today 47 (1999) 169.
- [3] S.C. Sorenson, J.W. Hoj, P. Stobbe, Flow Characteristics of SiC Diesel Particulate Filter Material, SAE Technical Paper 940236 (SP-1020), 1994.

- [4] A. Itoh, K. Shimato, T. Komori, H. Okazoe, T. Yamada, K. Niimura, Y. Watanabe, Study of SiC Application to Diesel Particulate Filter (Part 1): Material Development, SAE Technical Paper 930360 (SP-943), 1993.
- [5] A.G. Konstandopoulos, E. Papaioannou, D. Zarvalis, S. Skopa, P. Baltzopoulou, E. Kladopoulou, M. Kostoglou, S. Lorentzou Catalytic Filter Systems with Direct and Indirect Soot Oxidation Activity, SAE Technical Paper 2005-01-0670, 2005.
- [6] A.G. Konstandopoulos, D. Zarvalis, E. Papaioannou, N. D. Vlachos, G. Boretto, M.F. Pidria, P. Faraldi, O. Piacenza, P. Prenninger, T. Cartus, H. Schreier, W. Brandstatter, C. Wassermayr, G. Lepperhof, V. Scholz, B. Luers, J. Schnitzler, M. Claussen, A. Wollmann, M. Maly, G. Tsotridis, B. M. Vaglieco, S.S. Merola, D. Webster, D. Bergeal, C. Gorsmann, H. Obernosterer, D. Fino, N. Russo, G. Saracco, V. Specchia, N. Moral, A. D'Anna, A. D'Alessio, R. Zahoransky, E. Laile, S. Schmidt, M. Ranalli, The Diesel Exhaust Aftertreatment (DEXA) Cluster: A Systematic Approach to Diesel Particulate Emission Control in Europe, SAE Technical Paper No. 2004-01-0694 (SP-1861), 2004.
- [7] T. Fend, B. Hoffschmidt, R. Pitz-Paal, O. Reutter, P. Rietbrock, Energy 29 (5–6) (2004) 823.
- [8] T. Fend, R. Pitz-Paal, O. Reutter, J. Bauer, B. Hoffschmidt, Sol. Energy Mater. Sol. Cells 84 (2004) 291.
- [9] A.R. de Arrelano-Lopez, J. Martinez-Fernandez, P. Gonzalez, C. Dominguez, V. Fernandez-Quero, M. Singh, Int. J. Appl. Ceram. Technol. 1 (1) (2004) 56.
- [10] B. Hoffschmidt, V. Fernández, A.G. Konstandopoulos, I. Mavroidis, M. Romero, P. Stobbe, F. Téllez, Development of ceramic volumetric receiver technology, in: K.H. Funken, W. Bucher (Eds.), Proceedings of Fifth Cologne Solar Symposium, DLR, Germany, 2001, pp. 51–61.
- [11] B. Hoffschmidt, V. Fernández, R. Pitz-Paal, M. Romero, P. Stobbe, F. Téllez, The development strategy of the HiTREC volumetric receiver technology—up-scaling from 200 kWh via 3 MWh up to 10 MWel, in: Proceedings of the 11th SolarPACES International Symposium on Concentrated Solar Power and Chemical Energy, Technologies, Zürich, Switzerland, September 2002.
- [12] F. Tellez, M. Romero, P. Heller, A. Valverde, J.F. Reche, S. Ulmer, G. Dibowski, Thermal performance of “SolAir 3000 kWh” ceramic volumetric solar receiver, in: Proceedings of 11th SolarPACES International Symposium on Concentrated Solar Power and Chemical Energy, Technologies, Zürich, Switzerland, September 2002.
- [13] D.J. Green, An Introduction to the Mechanical Properties of Ceramics, Cambridge University Press, Cambridge, 1998.
- [14] Engineered Materials Handbook, Ceramics and Glasses, vol. 4, ASM International, The Materials Information Society, 1991.
- [15] S. Sarva, S. Nemat-Nasser, Mater. Sci. Eng. A 317 (2001) 140.
- [16] R.K. Govila, J. Mater. Sci. 19 (1984) 2111–2120.
- [17] S. Dutta, J. Am. Ceram. Soc. 71 (11) (1988) C-474.
- [18] C.B. Lim, T. Iseki, J. Mater. Sci. 25 (1990) 4203.
- [19] D.P. Butt, R.E. Tressler, K.E. Spear, J. Am. Ceram. Soc. 75 (12) (1992) 3268.
- [20] K. Breder, V.J. Tennery, J. Eur. Ceram. Soc. 17 (1997) 1579.
- [21] L.J. Gibson, M.F. Ashby, Cellular Solids—Structure and Properties, Cambridge University Press, Cambridge, 1997.
- [22] K. Ohno, K. Shimato, N. Taoka, H. Santae, T. Ninomiya, T. Komori, O. Salvat, Characterization of SiC-DPF for passenger car, SAE Technical Paper No. 2000-01-0185 (SP-1497), 2000.
- [23] S. Miwa, F. Abe, T. Hamanaka, Y. Miyairi, Diesel particulate filters made of newly developed SiC, SAE Technical Paper No. 2001-01-0192 (SP-1582), 2001.
- [24] M. Harada, S. Ichikawa, A. Otsuka, M. Hattori, S. Hashimoto, Durability Study on Si-SiC Material for DPF, SAE Technical Paper No. 2005-01-0582, 2005.
- [25] W.A. Cutler, G.A. Merkel, A New High Temperature Ceramic Material For Diesel Particulate Filter Applications, SAE Technical Paper No. 2000-01-2844, 2000.
- [26] N. Miyakawa, H. Maeno, H. Takahasi, Characteristics and Evaluation of Porous silicon Nitride DPF, SAE Technical Paper No. 2003-01-0386, 2001.
- [27] C.G. Li, F. Mao, S.B. Swartzmiller, S.A. Wallin, R.R. Ziebarth, Properties and Performance of Diesel Particulate Filters of an Advanced Ceramic Material, SAE Technical Paper No. 2004-01-0955, 2004.
- [28] S. Sugiyama, M. Togaya, J. Am. Ceram. Soc. 84 (12) (2001) 3013.
- [29] N.S. Jacobson, J. Am. Ceram. Soc. 76 (1) (1993) 3.
- [30] S. Palero, M. Romero, J.L. Castillo, Comparison of experimental and numerical air temperature distributions behind a cylindrical volumetric solar absorber module, in: Proceedings of 13th SolarPACES International Symposium on Concentrated Solar Power and Chemical Energy Technologies, Seville, Spain, June 2006.
- [31] C. Agrafiotis, M. Roeb, A.G. Konstandopoulos, L. Nalbandian, V.T. Zaspalis, C. Sattler, P. Stobbe, A.M. Steele, Sol. Energy 79 (4) (2005) 409.
- [32] M. Roeb, C. Sattler, R. Klüser, N. Monnerie, L. de Oliveira, A.G. Konstandopoulos, C. Agrafiotis, V.T. Zaspalis, L. Nalbandian P. Stobbe, A.M. Steele, J. Sol. Energy Eng.—Trans. ASME 128 (2006) 125.